Journal of
Applied Crystallography
ISSN 0021-8898

Received 19 March 2005
Accepted 24 May 2005

Energy calibration and full-pattern refinement for strain analysis using energy-dispersive and monochromatic X-ray diffraction

J. Liu,[a] K. Kim,[a] M. Golshan,[b] D. Laundy[b] and A. M. Korsunsky[a]*

[a]Department of Engineering Science, University of Oxford, Parks Road, Oxford OX1 3PJ, UK, and [b]Synchrotron Radiation Department, Daresbury Laboratory, Warrington WA4 4AD, UK. Correspondence e-mail: alexander.korsunsky@eng.ox.ac.uk

Precise channel-to-energy conversion is very important in full-pattern refinement in energy-dispersive X-ray diffraction. Careful examination shows that the channel-to-energy conversion is not entirely linear, which presents an obstacle to obtaining accurate quantitative data for lattice strains by pattern refinement. In order to establish an accurate quadratic channel-to-energy conversion function, a *Matlab* program was written to find the best quadratic coefficient and hence the whole energy conversion function. Then this energy conversion function was used to perform a whole-pattern fitting of the energy-dispersive X-ray diffraction pattern of a Ti64 sample. The strain across the Ti64 bar calculated from the fitting results has been compared with values obtained by single-wavelength X-ray diffraction utilizing a Laue monochromator.

1. Introduction

Diffraction of penetrating radiation such as neutrons or high-energy X-rays provides a powerful non-destructive method of interrogating the details of crystal lattice structures in the bulk of metallic alloy polycrystals. By collecting individual diffraction peaks or entire sections of diffraction patterns, it is possible to obtain information about residual micro- and macrostrain as well as grain orientation (texture).

There are two principal methods of recording diffraction patterns in use: the monochromatic beam angle-dispersive technique, and the white-beam energy-dispersive technique. Of the two methods, the monochromatic beam technique is more widely used, both in the laboratory setting and at synchrotron beamlines. The principal advantage of the monochromatic method is the high resolution of peak centre position and peak shape. The main disadvantage of this technique is associated with the necessity of scanning the detector over a range of angles to obtain a pattern, although the use of position-sensitive detectors (PSDs) serves to reduce the measurement time. In addition, information about the macroscopic strain obtained from a single diffraction peak is susceptible to errors associated with the inhomogeneity of elasto-plastic deformation between grains (Clausen *et al.*, 2003). Furthermore, the number of grains may be small that lie within the sampling volume and are in the diffraction condition, thus contributing to a peak. Apart from the total flux from the source, the intensity of the observed peak depends on the degree of monochromation (energy bandwidth) and the selectivity of the beam in terms of grain orientation. At synchrotron beamlines, these parameters are particularly high, due to the very low divergence of the beam and good optics. When engineering applications are considered, often macroscopic averages are sought, and this high selectivity may be a disadvantage. A preferred solution would be to use a monochromator system that offers an energy bandpass in the region of $\Delta E/E = 10^{-3}$, and may allow the divergence of the beam to be somewhat increased, so that a larger number of grains contribute to each reflection, thus improving the counting statistics.

A high-energy Laue monochromator system has recently been proposed and implemented on Station 16.3 at Daresbury by Laundy *et al.* (2004). A silicon crystal monochromator is mounted to produce a small bouncing angle in the transmission geometry, and is bent sagittally. Sagittal bending induces a spread of lattice parameters within the crystal, thus increasing the bandpass but decreasing the quality of monochromation within a reasonable range, while at the same time producing some focusing (and hence divergence) in the horizontal plane.

The second method used in the present study is the white-beam energy-dispersive technique. This method allows very fast data collection times for the entire pattern over a large range of lattice spacings. However, the procedures for pattern interpretation and refinement still require some development. Several examples of interpretation procedures have been developed in an *ad hoc* fashion for specific purposes by several authors. In dealing with energy-dispersive diffraction data acquired from a laboratory X-ray source, Ballirano & Caminiti (2001) transformed the data to the angular dispersive domain for full-pattern refinement. Similarly, Steuwer *et al.* (2004) developed an approach involving the transformation of data into a format of time-of-flight neutron diffraction, and used this approach for their strain mapping investigation using energy-dispersive synchrotron X-ray diffraction. The real

predicament, however, is the fact that accurate pattern refinement is usually hampered by a small degree of non-linearity in the conversion between channel numbers and photon energies. This non-linearity has also been noted by Dong *et al.* (2003), who proposed an algorithm for full-pattern refinement that deals with non-linearity and errors in energy measurements, especially for high-pressure energy-dispersive X-ray diffraction studies. In our approach, we assume that this non-linearity can be adequately represented by a quadratic term, and propose a procedure allowing the coefficients in the quadratic conversion function to be determined using a pattern from a well characterized powder sample, such as the NIST silicon standard, as calibrant. The solution that we propose is therefore comparatively general, and could be used in the context of any application of energy-dispersive X-ray diffraction when accurate calibration of the channel-to-energy conversion is required.

The purpose of the set of experiments described in the present paper was to investigate the application to the analysis of lattice strains in engineering materials and components of two experimental techniques: high-energy single-bounce Laue monochromatic beam diffraction, and white-beam energy-dispersive diffraction.

Strain determination by diffraction for the purposes of stress evaluation is a well established branch of diffractometry, represented in a large body of literature (Cullity, 1978; Noyan & Cohen, 1987; Hauk, 1997). The most widely used method of analysis documented in this literature concerns the $\sin^2\psi$ method, which involves the collection of multiple peak positions for different orientations of the scattering vector with respect to the sample, and the determination of the underlying state of stress from these measurements. It is important to note that the subject of the present paper is very different from this conventional approach in several important respects. Firstly, no attempt is made to collect data from the sample position (gauge volume) within the sample for several different orientations of the scattering vector. Rather, the orientation of the scattering vector with respect to the sample is kept fixed, but the gauge volume position is changed, thereby allowing the spatial variation of a strain component to be worked out. Secondly, since all measurements are carried out with high-energy X-rays and in transmission, no corrections for absorption are needed, and direct access to bulk strain measurement is gained.

As an example of an engineering material possessing considerable practical importance for aerospace and other structural applications, a two-phase near-alpha titanium alloy, Ti–6Al–4V, was chosen. The predominant alpha phase in this material has a hexagonal close packed (h.c.p.) structure, and gives rise to a large number of peaks in the diffraction pattern. One of the interesting aspects of the deformation behaviour of this material is the anisotropy of elastic and plastic properties with respect to the direction within the hexagonal lattice cell. For example, slip systems exhibiting easy slip are associated with the basal {00.1} plane and close packed [11.0] directions, while easy elastic deformation (lowest elastic modulus) corresponds to the *c*-axis direction, [00.1]. Detailed characterization of lattice strains in titanium alloys often requires separate evaluation of lattice strains that correspond to the *a* axis and *c* axis and other specific orientations, but also the evaluation of overall macroscopic average strains. We demonstrate that the two experimental methods considered in the present paper (Laue monochromation and energy-dispersive diffraction) are well suited to the task, and show excellent agreement between the results.

2. Experimental details and data analysis

Two experiments on monochromatic and white-beam synchrotron X-ray diffraction in transmission through a bent bar of Ti–6Al–4V titanium alloy were carried out on Station 16.3 (Collins *et al.*, 1999) at SRS, Daresbury Laboratory, UK. The specimen of Ti64 was machined to the dimensions h_y = 50 mm, h_x = 8.5 mm, h_z = 4 mm, and bent by applying a bending moment M_z of approximately 100 N m using a universal testing machine with a four-point bending attachment. A monochromatic X-ray beam with energy of about 68 keV produced by a Laue monochromator (Laundy *et al.*, 2004) was used in the first experiment. In the second experiment, the same bent bar was studied using the white (polychromatic) beam and an energy-dispersive detector.

In the Laue monochromatic setup, a singe bent silicon single crystal was placed at a small angle from the vertical in the path of the incident beam to produce a transmitted monochromatic X-ray beam. The direction of the transmitted monochromatic beam formed an angle of about 6° with the incident beam, and the energy of the monochromatic beam was 68 keV. The monochromator crystal was bent to select a bandwidth in the range of $\Delta E/E$ between 10^{-4} and 10^{-3}, allowing the degree of monochromation to be readily adjusted to match the properties of the object. Beam size used in the experiment was 0.2 mm in the vertical direction and 0.2 mm in the horizontal direction. Peak centre positions were obtained by fitting Gaussian, pseudo-Voigtian or combined peak shapes to the observed diffraction peaks.

In the white-beam experiment, the experimental setup was similar to that described by Korsunsky *et al.* (2002). The scattering angle was fixed at 10°. Diffraction patterns of the standard calibrant silicon powder and at different position within the bent titanium alloy bar were recorded. The data were then analysed by performing Rietveld refinement using the *General Structure Analysis System*, *GSAS* (Larson & Von Dreele, 2000), with the graphical user interface *EXPGUI* (Toby, 2001). The Pawley (1981) refinement approach was used in the data analysis.

The channel-to-energy conversion was initially calibrated using a radioactive source (Am^{209}) and assumed to be linear. Careful examination, however, shows that the energy conversion is not entirely linear. This presents an obstacle to obtaining accurate quantitative data for lattice strains by pattern refinement. The following procedure was adopted in order to establish an accurate quadratic channel-to-energy conversion function. Firstly, the sign and range of variation of the coefficient of the quadratic term was identified by running

a few tests with *GSAS*: when the quadratic coefficient is set to be too large, the quality of fit deteriorates. In order to find the best value of the coefficient within the selected range, a *Matlab* program was written. The program performed data preparation for *GSAS* by prepending a header containing a particular quadratic energy-conversion function to the data file, and launched *GSAS* refinement of the silicon power pattern. After the chosen number of iterations, *GSAS* produced an output file containing, amongst other data, the quality of fit parameter R_p. The *Matlab* program performed this procedure for the chosen set of values of the quadratic term coefficient, and generated output in the form of a table of fit quality *versus* quadratic term coefficient. The program could be run repeatedly in order to obtain the best value of the quadratic term coefficient to the desired precision. Once this value was determined, the quadratic channel-to-energy conversion function was used throughout the analysis of all data obtained from the titanium alloy bent bar.

It is clear that implementing the channel-to-energy calibration procedure outside the *GSAS* framework is an inefficient step. The task of finding the best calibration would be better accomplished by incorporating this procedure within the *GSAS* package, which, after all, is devised for non-linear optimization.

A second *Matlab* program was written to perform full-pattern fitting of the data sets one by one, starting from an example refinement that was manually fitted. Then the program generated output of the results of lattice parameters for all the data sets.

3. Results and discussion

The initial linear fitting of channel-to-energy conversion from the radiation source is shown in Fig. 1(*a*), in which the linear equation is also shown. Two W characteristic radiations (energy and channel) and one Am characteristic radiation (energy and channel) are used initially to calibrate the channel-to-energy conversion.

The diffraction data collected in energy-dispersive mode are counts *versus* channel numbers, then the linear channel-to-energy conversion is used to convert channel numbers to X-ray energies (keV). The Si diffraction data were then transferred into *GSAS* format and input into *GSAS*. The experimental and refined Si patterns are shown in Fig. 2(*a*). The '+' marks correspond to the experimental pattern that is obtained with the help of the channel-to-energy conversion, while the solid line is the calculated pattern using the lattice parameter of the Si standard. The positions of the diffraction peaks are also marked, and the difference between the experimental and calculated patterns is shown at the bottom. The fitting is basically fine, but careful examination of the difference line shows that the peak positions are not accurate enough. The position of peak 220 at 37.114 keV is completely correct, but the other peak positions are not so accurate. The

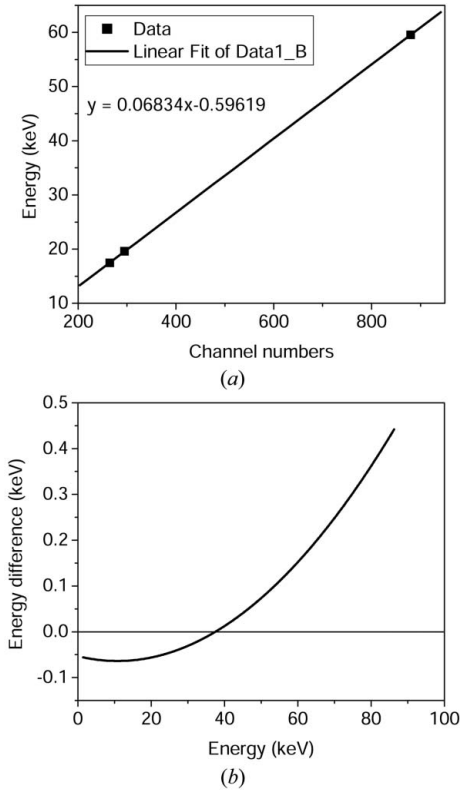

Figure 1
(*a*) Linear calibration of channel-to-energy conversion from W and Am radiation source. (*b*) Energy difference between quadratic and linear channel-to-energy conversion.

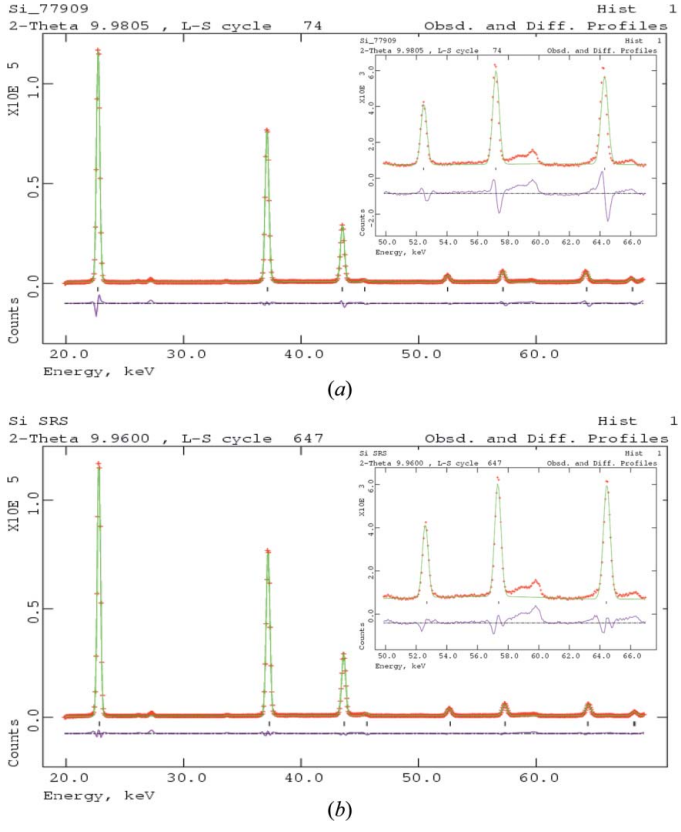

Figure 2
Fitted Si powder patterns using *GSAS*: (*a*) linear energy conversion, (*b*) quadratic energy conversion.

experimental peak 111 at 22.728 keV is shifted to the right of the calculated position, whereas the experimental peaks at energies higher than 40 keV are shifted to the left of the calculated positions. This means that the linear channel-to-energy conversion is not strictly correct. There should be a quadratic term in the energy conversion equation, which can correct the discrepancies between the experimental pattern and the calculated pattern.

The *Matlab* program was run to obtain the best fit of the Si diffraction data; thus the quadratic channel-to-energy conversion coefficients were optimized. The best fit of the Si patterns is shown in Fig. 2(*b*). It can be seen that the fitting of peak positions is much better than in Fig. 2(*a*). Compared with the peak positions in Fig. 2(*a*), the experimental peaks in Fig. 2(*b*) are shifted to lower energies in the low-energy range, and those at high energies are shifted to higher energies. The experimental position and intensity of every peak coincides perfectly with those calculated.

In the particular case considered, the quadratic function for channel-to-energy conversion that provides the best quality of fit is given by

$$E = -0.648 + 0.0682N + 4.202 \times 10^{-7}N^2, \qquad (1)$$

where E denotes photon energy (in keV) and N represents the channel number.

The energy difference between the quadratic and the linear channel-to-energy conversion is shown in Fig. 1(*b*). The abscissa is the X-ray energy in keV, while the ordinate shows the energy difference. It shows that at around 38 keV, the quadratic and linear conversions have the same energy; in the energy range below 38 keV, the energy in the quadratic conversion is lower than that in the linear conversion, whereas in the energy range above 38 keV, the energy in the quadratic conversion is higher. This is consistent with what has been observed in Figs. 2(*a*) and 2(*b*).

Ti–6Al–4V is an alloy that is widely used to manufacture components located at the front of the aeroengine, such as fan blades and disks. The structure achieved by the manufacturing process is obtained by solution treating in the middle of the α+β phase field and air cooling. This gives a mixture of primary alpha and a transformation product which comprises α and β phases. The α phase has an h.c.p. structure which is typical of titanium at room temperature and transforms to a body centred cubic (b.c.c.) structure, the cubic β phase, at 1156 K.

The b.c.c. β phase is not contiguous and occupies 'islands' surrounded by the predominant h.c.p. α phase, which at room temperature deforms mainly by basal slip and imposes a strong constraint on the β phase. As a consequence of this two-phase structure, large strains are often observed within the minority phase, which is constrained within the matrix of the major phase. Other modifications of titanium lattice structure, particularly the orthorhombic phase, may also be present.

A bar of Ti–6Al–4V alloy with dimensions h_y = 50 mm, h_x = 8.5 mm, h_z = 4 mm was machined from a plate. Preferred orientation in the bar was evaluated using laboratory X-ray diffraction using a Bruker AXS D8 diffractometer with Euler cradle. Texture was found not to be significantly high (not exceeding 2× random), so the material was thought to be untextured. The bar was bent by applying a bending moment M_z of approximately 100 N m using a universal testing machine with a four point bending attachment, Fig. 3(*a*). Lines labelled A, B and C in Fig. 3(*a*) illustrate the stress profiles that correspond to progressively increasing applied bending moment (for the case of non-work-hardening material). At the instant when the applied moment just reaches the critical value required for yielding, the stress (and elastic strain) distribution across the bar is linear (line A). When the applied moment is increased further (line B), the material undergoes progressive plastic yielding, beginning at the surface. The total strain remains linear across the beam, but a proportion of it is now accommodated plastically. As the moment is increased further (line C), so does the zone of plasticity. Upon unloading, the residual elastic strain profile has the 'z' shape illustrated in Fig. 3(*b*).

The residually stressed bent bar of Ti–6Al–4V alloy was scanned through the beam, and patterns recorded and refined

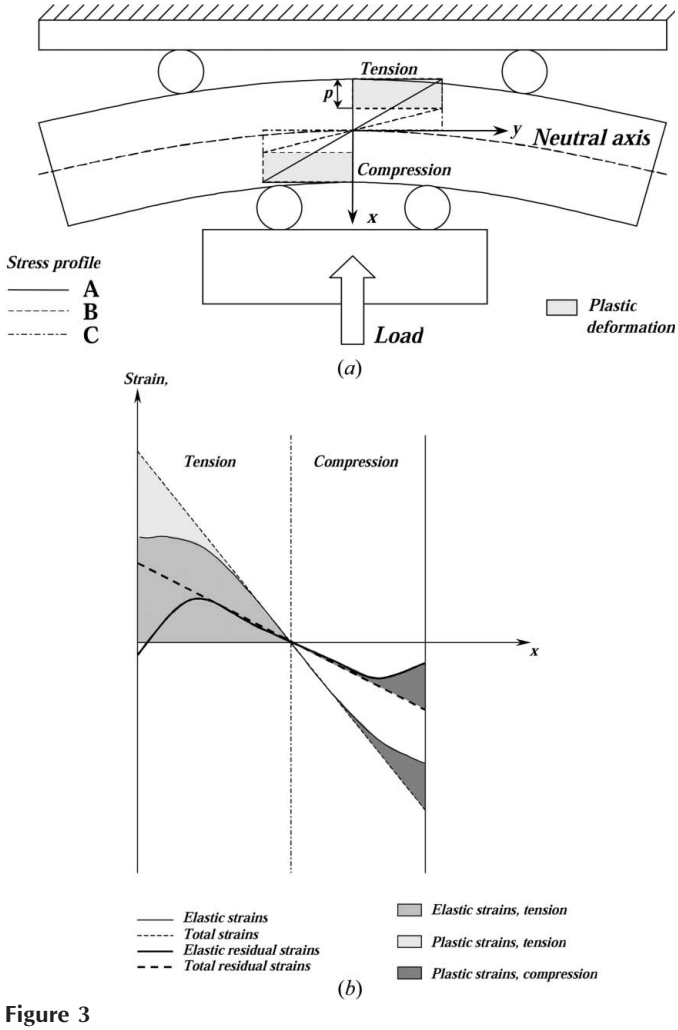

Figure 3
(*a*) Illustration of the bending experiment used to generate the residual stress profile within the sample. (*b*) Illustration of the residual stress (and residual elastic strain) profile across the bent sample.

in order to investigate the state of strain within gauge volumes along this line. A representative diffraction pattern of the Ti alloy was put into *GSAS*, and lattice parameters and peak profile coefficients were refined to a satisfactory quality. Then a *Matlab* program was used to run *GSAS* in batch mode to fit the Ti alloy diffraction patterns one by one, to produce the resulting lattice parameters. The relative error obtained from the *GSAS* refinement is around 0.66×10^{-4} for lattice parameter '*a*', around 1.05×10^{-4} for lattice parameter '*c*' of the h.c.p. α phase, and up to 2×10^{-4} for lattice parameters of the other phases.

With the help of correct quadratic channel-to-energy conversion, careful examination of the state of strain within polycrystalline multiphase materials can be undertaken. Two examples of refined Ti-alloy patterns are shown in Figs. 4(*a*) and 4(*b*). The bottom line of markers indicates the peak positions of the Ti α phase, the middle line of markers are for Ti β phase, and the top line of markers for the orthorhombic phase. Comparison between the two patterns reveals that one of the peaks corresponding to the Ti β phase, 310, shows particular sensitivity to the deformation state: it is clearly present in the pattern in Fig. 4(*a*), but absent in Fig. 4(*b*). Detailed analysis of the data reveals that this peak is only present in the regions within the sample that are subjected to tensile residual stress, but absent where the stress is compressive.

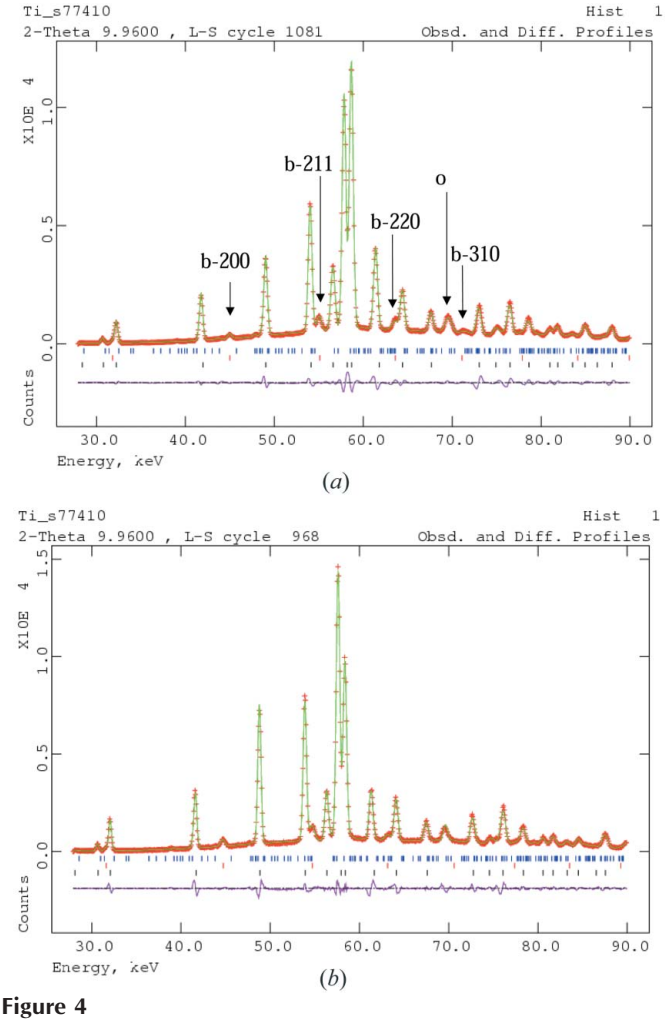

Figure 4
(*a*) X-ray diffraction pattern of Ti–6Al–4V alloy refined using the newly proposed calibration procedure. Peaks of the minority phases, the b.c.c. β (denoted by 'b') and the orthorhombic phase (denoted by 'o') are indicated. Note the presence of the small 310 peak of the β phase. (*b*) X-ray diffraction pattern of Ti–6Al–4V alloy refined using the newly proposed calibration procedure, obtained from a different location within the sample. The 310 peak of the β phase is absent from this pattern.

A general observation ought to be made here on the interpretation of diffraction patterns of *in situ* loaded or residually stressed volumes of polycrystals. The distinction between powder patterns and coherent polycrystalline solids must be made first. Powders can usually be safely assumed to be free from macroscopic stress and strain, unlike polycrystalline solids. In a polycrystal, loading induces strains in grains of all orientations. However, only grains contributing to the diffraction pattern are those containing 'allowed' lattice planes lying normal to the scattering vector. Strictly speaking, uniaxial strain loading of a lattice cell induces a distortion, rather than a change in the lattice parameter. It must also be noted that all crystal orientations obtained by rotation around the scattering vector contribute to the diffraction signal, although their strain states may actually differ. Finally, it is important to note that elastic strains involved are usually too small to produce detectable peak splitting.

Precise evaluation of diffraction peak positions in terms of energy (in white-beam studies) or diffraction angle (in monochromatic beam studies) allows lattice strain in the scattering vector direction to be computed (see below). However, it is important to note that in many cases the purpose of diffraction measurement is to evaluate the stress state within the gauge volume, rather than strain. This task requires the knowledge and understanding of the nature of microscopic (single grain) and macroscopic (polycrystalline) stiffness matrices, and making certain assumptions about the full three-dimensional deformation state. This is in many ways the weakest link in the analysis, and is prone to errors. However, in the present paper we do not concern ourselves with this problem at all: our attention is confined to the analysis of strains.

Consider a situation where elastic anisotropy (*i.e.* the dependence of stiffness on grain orientation) is negligible. This means that, under elastic conditions, the strain that arises in all grains is the same. Considering a cubic structure for simplicity (without restricting the generality of the argument) and denoting the strain by *e*, we obtain the new lattice spacing for a set of planes *hkl* given by

$$d_{hkl} = (1 + e)d^0_{hkl} = (1 + e)a_0/f_{hkl}, \qquad (2)$$

where

$$f_{hkl} = (h^2 + k^2 + l^2)^{1/2}.$$

Although the lattice may also undergo expansion or contraction in the direction perpendicular to the scattering vector, this phenomenon does not affect the Bragg peak position in the present diffraction experiment. Equation (2) holds for all peaks within one diffraction pattern, and can be written as

$$d_{hkl} = (1 + e)d^0_{hkl} = a^e/f_{hkl}, \quad (3)$$

where a^e is now used to denote a 'strained' lattice parameter.

The above discussion demonstrates that the observed diffraction pattern appears to be exactly such as if it is the lattice parameter that has experienced strain e, *i.e.*

$$a^e = (1 + e)a^0. \quad (4)$$

The above conclusion can be generalized for the h.c.p. lattice, in which case separate strain values e_a and e_c must be introduced for the two lattice parameters.

The above argument demonstrates why it has become conventional in diffraction strain analysis to use Rietveld refinement in the same way as one would for a powder sample, and associate strain with lattice parameter change, rather than cell distortion. From the large body of literature available on the subject, we refer to the paper by Daymond *et al.* (1999) for the discussion of this issue. It is important to note that experimental validation of this approach has shown excellent accuracy and agreement with the applied macroscopic average elastic strain.

Based on quadratic channel-to-energy calibration of the detector, pattern refinement was carried out for the determination of lattice parameters, producing the fits illustrated in Fig. 4. Once the lattice parameters were found, corresponding strains were computed on the basis of each parameter by rearranging equation (4) into the form

$$e = (a^e/a^0) - 1. \quad (5)$$

It is important to note that, contrary to the simplifying assumption made above about uniformity of strain with orientation (isotropy), in practice elastic strains differ depending on the orientation of diffracting lattice planes within the unit cell. As a consequence, a situation arises where individual peaks are shifted with respect to the their 'regular' positions that might be expected for a powder sample. It is now well established that orientation dependence of elastic and plastic deformation of grains within polycrystalline aggregates results in the development of so-called 'anisotropy', or 'difference strains' (*e.g.* Korsunsky *et al.*, 2002). These terms refer to the apparent inconsistency in the strains (and hence peak positions) observed for different reflections. This leads to a problem in the refinement of diffraction patterns, and apparent degradation of the quality of fit. Some *ad hoc* measures have been proposed to overcome this difficulty (Daymond *et al.*, 1999). They consist of introducing an additional parameter (anisotropy strain) in the Rietveld refinement that provides a measure of how much each peak is displaced from its position. However, since these displacements are prescribed solely in accordance with the elastic stiffness variation with lattice orientation, the approach fails to deal efficiently with the consequences of plastic anisotropy of the single crystals that constitute the aggregate.

This situation is clearly reflected in the *GSAS* fit of the Ti64 alloy in the present case. In Fig. 4, peak positions for the Ti α and Ti β phases manifest visible 'anisotropy strain' behaviour, with peak positions showing displacements (of opposite sign) with respect to their predicted positions. This observation has interesting and important implications for the internal stress state of two-phase titanium alloys. The results of our study of this phenomenon will be reported separately.

Figs. 5(*a*) and 5(*b*) show the comparison of strain across the scanned line of the Ti alloy bar between the Laue monochromatic beam method and energy-dispersive white-beam method. The strain in the white-beam method is calculated from the lattice parameters produced by *GSAS* whole-pattern fitting, while the strain in the Laue monochromation method is calculated from the peak positions obtained from a single peak fitted using a Gaussian peak shape. The strain calculated from white-beam lattice parameter '*a*' and the strain determined from the monochromatic 110 peak are compared in Fig. 5(*a*), while the strains from the white-beam lattice parameter '*c*' and from the monochromatic 002 peak are shown in Fig. 5(*b*). The strain shows a typical bending profile of the central line of bending. It can be seen that the strains from both methods match very well, which means that both methods are successful.

The current example provides an excellent vehicle to illustrate the level of detail afforded by white-beam energy-dispersive analysis. Although the b.c.c. β phase and the

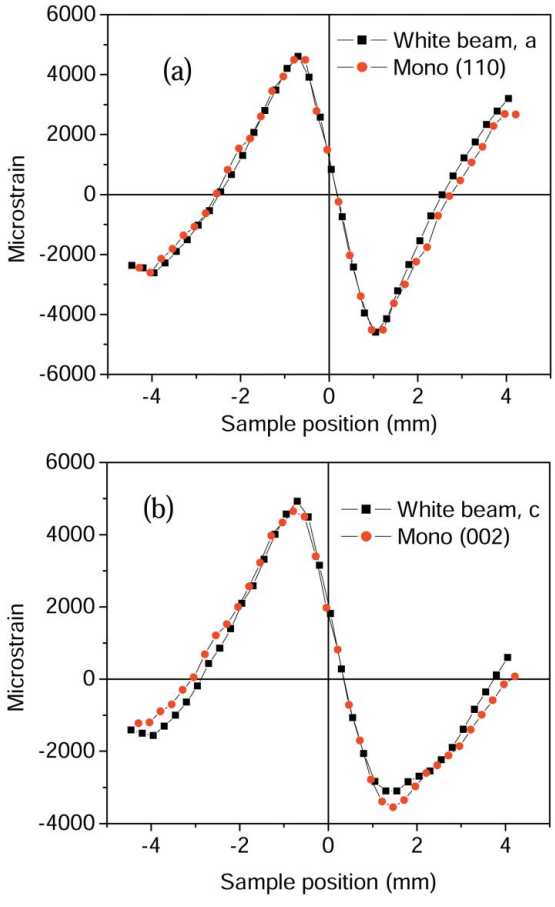

Figure 5
Comparison of strain determined by monochromatic and white-beam X-ray diffraction: (*a*) lattice parameter *a* from white-beam diffraction and peak 110 from monochromatic diffraction, (*b*) lattice parameter *c* from white-beam diffraction and peak 002 from monochromatic diffraction.

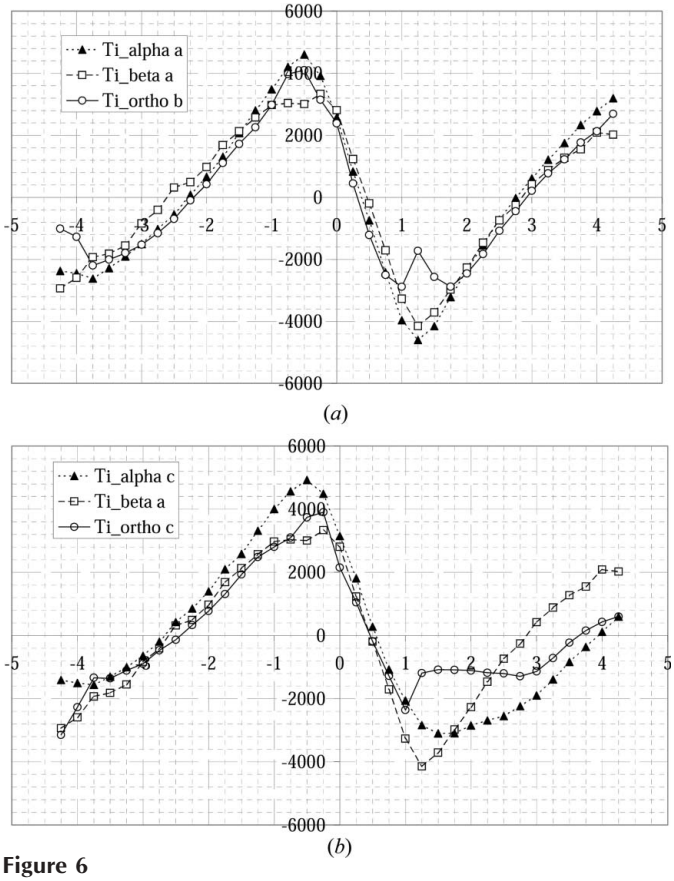

Figure 6
(*a*) Comparison of strain profiles calculated on the basis of different lattice parameters: *a* of the h.c.p. α phase, *a* of the b.c.c. β phase, and *b* of the orthorhombic phase. Good agreement is observed between all three cases. (*b*) Comparison of strain profiles calculated on the basis of different lattice parameters: *c* of the h.c.p. α phase, *a* of the b.c.c. β phase, and *c* of the orthorhombic phase. The behaviour of strain associated with the *c* parameter of the orthorhombic phase most closely follows that of *a* of the b.c.c. β phase.

orthorhombic phase are minority phases, probably amounting to less than 10% of the material, excellent lattice parameter evaluation is also possible for these phases.

Fig. 6(*a*) shows a comparison between strain profiles calculated on the basis of the lattice parameter *a* of the h.c.p. α phase, *a* of the b.c.c. β phase, and *b* of the orthorhombic phase. Good agreement is observed between all three cases.

Fig. 6(*b*) shows a comparison of strain profiles calculated on the basis of the lattice parameter *c* of the h.c.p. α phase, *a* of the b.c.c. β phase, and *c* of the orthorhombic phase. The behaviour of strain associated with the *c* parameter of the orthorhombic phase most closely follows that of *a* of the b.c.c. β phase.

4. Conclusion

A rational procedure was developed, and a *Matlab* program implementing it was written, with the objective of finding the best form of quadratic channel-to-energy number conversion for an energy-dispersive diffraction detector, by fitting the energy-dispersive X-ray diffraction pattern of the standard Si powder. Hence, adequate accuracy of peak placement was achieved across the entire energy spectrum considered. The use of a quadratic energy conversion function was compared with an approximate linear energy conversion function, and was found to improve substantially the quality of pattern refinement, and hence interpretation. Then the quadratic energy conversion function was used to perform pattern refinement of energy-dispersive X-ray diffraction patterns of a bent titanium alloy sample. Strain distributions extracted from monochromatic and white-beam experiments were found to be in good agreement. Furthermore, detailed analysis of the deformation state within each of the three phases present was also possible.

References

Ballirano, P. & Caminiti, R. (2001). *J. Appl. Cryst.* **34**, 757–762.
Clausen, B., Leffers, T. & Lorentzen, T. (2003). *Acta Mater.* **51**, 6181–6188.
Collins, S. P., Murphy, B. M., Tang, C. C., Miller, M. C. & Oszlanyi, G. (1999). *J. Phys. D Appl. Phys.* **32**, A81–A83.
Cullity, B. D. (1978). *Elements of X-ray Diffraction.* New York: Addison-Wesley.
Daymond, M. R., Bourke, M. A. M. & Von Dreele, R. B. (1999). *J. Appl. Phys.* **85**, 739–747.
Dong, Y. H., Liu, J., Li, Y. C. & Li, X. D. (2003). *J. Appl. Cryst.* **36**, 1123–1127.
Hauk, V. (1997). Editor. *Structural and Residual Stress Analysis by Non-destructive Methods: Evaluation, Application, Assessment.* Amsterdam: Elsevier.
Korsunsky, A. M., Collins, S. P., Owen, R. A., Daymond, M. R., Achtioui, S. & James, K. E. (2002). *J. Synchrotron Rad.* **9**, 77–81.
Korsunsky, A. M., Daymond, M. R. & James, K. E. (2002). *Mater. Sci. Eng. A*, **334**, 41–48.
Larson, A. C. & Von Dreele, R. B. (2000). *General Structure Analysis System* (*GSAS*), Los Alamos National Laboratory Report LAUR 86-748.
Laundy, D., Lennie, A., Golshan, M., Taylor, D., Roberts, M., Bushnell-Wye, G., Cernik, R., Flaherty, J. & Burrows, I. (2004). *AIP Conf. Proc.* **705**, 683.
Noyan, I. C. & Cohen, J. B. (1987). *Residual Stress: Measurement by Diffraction and Interpretation.* Berlin: Springer-Verlag.
Pawley, G. S. (1981). *J. Appl. Cryst.* **14**, 357–361.
Steuwer, A., Santisteban, J. R., Turski, M., Withers, P. J. & Buslaps, T. (2004). *J. Appl. Cryst.* **37**, 883–889.
Toby, B. H. (2001). *J. Appl. Cryst.* **34**, 210–213.